Chinese Journal of
POLYMER SCIENCE

ARTICLE

https://doi.org/10.1007/s10118-018-2096-9
Chinese J. Polym. Sci. 2018, 36, 417–424

BODIPY@Ir(III) Complexes Assembling Organic Nanoparticles for Enhanced Photodynamic Therapy

Yang Liu[a], Nan Song[a], Li Chen[a*], and Zhi-Gang Xie[b*]

[a] *Department of Chemistry, Northeast Normal University, Changchun 130024, China*
[b] *State Key Laboratory of Polymer Physics and Chemistry, Changchun Institute of Applied Chemistry, Chinese Academy of Sciences, Changchun 130022, China*

Electronic Supplementary Information

Abstract We present a new cyclometalated Ir(III) complexes IrBDP, which could self-assemble into organic nanoparticles (IrBDP NPs). IrBDP NPs show enhanced photodynamic effect and can be engulfed by HeLa cells for cell imaging as well as photodynamic therapy (PDT) upon low energy irradiation.

Keywords BODIPY; Photodynamic therapy; Iridium complex

Citation: Liu, Y.; Song, N.; Chen, L.; Xie, Z. G. BODIPY@Ir(III) Complexes Assembling Organic Nanoparticles for Enhanced Photodynamic Therapy. Chinese J. Polym. Sci. 2018, 36(3), 417–424.

INTRODUCTION

Photodynamic therapy (PDT), which is an approved medical technique for the treatment of malignant tissues, has attracted tremendous research interests[1–4]. Compared with chemotherapy, PDT possesses several advantages such as the minimal invasiveness, low toxicity, and spatial and temporal control[5–9]. For PDT, the singlet oxygen ($^1O_2$), which is the main agent for destroying cancer cells, is generated by the photosensitizer (PS) upon light irradiation. Up to now, the most commonly used PS for PDT is the hematoporphyrin derivatives[10–14]. Nevertheless, relatively poor reactive oxygen species (ROS) generation and low molar absorption coefficient limit the PDT efficacy for clinical uses. Alternatively, the boron dipyrromethene (BODIPY, BDP)[15, 16], a widely used fluorescence dye, was discovered to have potential photodynamic effect through the introduction of iodine[17–19] and Pt[20, 21] as well as forming dimer or trimer[22–26]. Compared with porphyrin systems, BDP as photosensitizers is in the bud, and less explored for their biological applications.

Cyclometalated Ir(III) complexes as efficient photosensitizers have been developed for PDT[27–30]. However, the absorbance mainly concentrated on the short wavelength region. To date, there are two methods to address this problem. One is developing Ir(III) complexes with two-photon absorption for ROS generation[31–35]. Another is combining the Ir(III) with the fluorescence dyes, such as aza-boron-dipyrromethene (aza-BDP)[36, 37] and BDP[38–41] because of their high molar absorption coefficient and good photostability. The combination of Ir(III) complexes and BDP is a great strategy to exert respective advantages, and results in enhanced synergistic effect.

In this work, we designed and synthesized fluorescent cyclometalated Ir(III) complexes containing BDP unit (IrBDP) in Scheme 1, which could self-assemble into corresponding organic nanoparticles (IrBDP NPs). The introduction of Ir(III) significantly increased the photodynamic effect of BDP. The cellular uptake and distribution of the IrBDP NPs were investigated by confocal laser scanning microscopy (CLSM). In addition, phototoxicity against murine colon cancer (CT26) and human cervical carcinoma (HeLa) cell line was validated. The live/dead staining experiment and cell apoptosis experiment also confirmed the potent cytotoxicity of IrBDP NPs upon irradiation.

EXPERIMENTAL

Materials

Solvents and reagents were purchased commercially as reagent grade and used as received unless otherwise mentioned. Dichloromethane (CH_2Cl_2) and 1,4-dioxane were distilled over calcium hydride. The solvents used for spectroscopic measurements were of HPLC grade.

Instruments

^{1}H-NMR spectra were recorded on a Bruker NMR 400 DRX Spectrometer using $CDCl_3$ as solvent. The mass spectra (MS) of the samples were recorded by the German company Bruker autoflex III smartbeam MALDI-TOF/TOF mass spectrometer

* Corresponding authors: E-mail chenl686@nenu.edu.cn (L.C.)
E-mail xiez@ciac.ac.cn (Z.G.X.)
Invited paper for special issue of "Supramolecular Self-Assembly"
Received September 27, 2017; Accepted November 23, 2017; Published online December 27, 2017

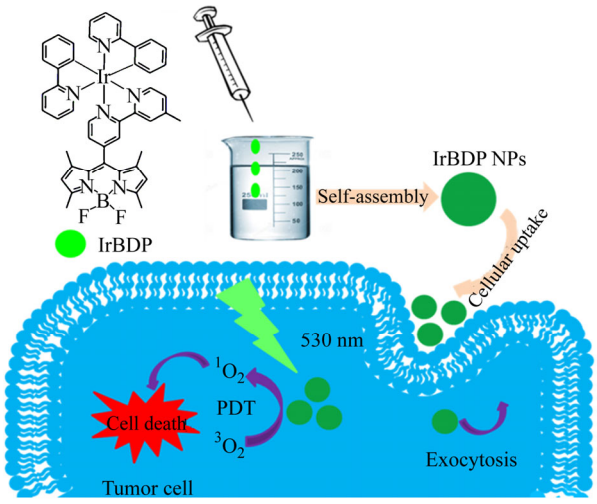

Scheme 1 The preparation of IrBDP NPs, cellular uptake and photodynamic therapy in cells

with smartbeam laser at 355 nm wavelength. UV-Vis absorption and emission measurement were carried on by using a Shimadzu UV-2450 PC UV-Vis spectrophotometer and a PerkinElmer LS-55 fluorescence spectrophotometer, respectively. Size and size distribution of the nanoparticles were determined by Malvern Zeta-Sizer Nano for dynamic light scattering (DLS). The morphology of the nanoparticles was measured by transmission electron microscopy (TEM) performed on a JEOL JEM-1011 electron microscope operating at an acceleration voltage of 100 kV. Confocal laser scanning microscopy (CLSM) images were taken using a Zeiss LSM 700 (Zurich, Switzerland).

Synthesis

Synthesis of compound ***a*** *(4'-methyl-[2,2'-bipyridine]-4-carbaldehyde)*

The compound **a** was synthesized according to the architecture. ^{1}H-NMR (400 MHz, $CDCl_3$, δ, ppm): 10.19 (s, 1H), 8.90 (d, J = 4.6 Hz, 1H), 8.84 (s, 1H), 8.58 (d, J = 4.7 Hz, 1H), 8.29 (s, 1H), 7.73 (d, J = 4.0 Hz, 1H), 7.20 (d, J = 4.2 Hz, 1H), 2.47 (s, 3H).

Synthesis of compound BDP (5,5-difluoro-1,3,7,9-tetramethyl-10-(4'-methyl-[2,2'-bipyridin]-4-yl)-5H-dipyrrolo[1,2-c:2',1'-f][1,3,2]diazaborinin-4-ium-5-uide)

The compound **a** (600 mg, 3 mmol) and 2,4-dimethyl-pyrrole (600 mg, 6 mmol) were dissolved in dry CH_2Cl_2 (200 mL) under N_2 atmosphere. To start the reaction, several drops of trifluoroacetic acid were added and the mixture was stirred for 5 days at room temperature. After 5 days, 2,3-dichloro-5,6-dicyano-1,4-benzoquinone (DDQ) (681 mg, 3 mmol) was added into the reaction and stirred for 4 h. Subsequently, TEA (5 mL, 36 mmol) and BF_3OEt_2 (6 mL, 48 mmol) were added into the reaction in ice-cold condition and stirred over night at room temperature. The mixture was washed with brine (100 mL). The organic layer was dried with anhydrous Na_2SO_4 and combined in vacuum. The residue was purified by silica chromatography using CH_2Cl_2/acetone (100/3, *V*/*V*) to afford the dark-red solid (250 mg, 20%). ^{1}H-NMR (400 MHz, $CDCl_3$, δ, ppm): 8.82 (dd, J = 4.8, 0.6 Hz, 1H), 8.51 (d, J = 4.9 Hz, 1H), 8.48 (s, 1H), 8.31 (s, 1H), 7.31 (dd, J = 4.9, 1.7 Hz, 1H), 7.17 (d, J = 4.9 Hz, 1H), 5.99 (s, 2H), 2.56 (s, 6H), 2.47 (s, 3H), 1.47 (s, 6H).

Synthesis of compound IrBDP

The compound BDP (0.24 mmol, 100 mg) and $[Ir(py)_2Cl]_2$ (0.1 mmol, 107.2 mg) were dissolved in 12 mL of mixed solution (CH_2Cl_2/MeOH, *V*/*V* = 2/1) and refluxed for 5 h under N_2 atmosphere. After 5 h, the mixture was cooled to room temperature, then NH_4PF_4 (200 mg) was added and stirred for 15 min. The solid was filtered and the filtrate was collected. Subsequently, the filtrate was evaporated in vacuum and the crude product was obtained, which was purified by column chromatography using EtOAc/CH_2Cl_2 (1/2, *V*/*V*) to afford red solid (35 mg, 16%). ^{1}H-NMR (400 MHz, $CDCl_3$, δ, ppm): 8.38 (s, 1H), 8.25 (s, 1H), 8.10 (d, J = 5.5 Hz, 1H), 7.95 (d, J = 8.1 Hz, 1H), 7.88 (d, J = 8.1 Hz, 1H), 7.83–7.66 (m, 6H), 7.62 (d, J = 5.5 Hz, 1H), 7.31 (dd, J = 5.5, 1.4 Hz, 1H), 7.24 (s, 1H), 7.14 (t, J = 6.6 Hz, 1H), 7.08–6.99 (m, 3H), 6.92 (t, J = 7.4 Hz, 2H), 6.34 (dd, J = 10.1, 7.9 Hz, 2H), 6.07 (s, 1H), 5.95 (s, 1H), 2.56 (s, 6H), 2.51 (s, 3H), 1.63 (s, 3H), 0.93 (s, 3H).

Synthesis of compound Ir-COOH

4-(2-Pyridyl)benzoic acid (compound **b**) (0.14 mmol, 28 mg) and $[Ir(py)_2Cl]_2$ (0.06 mmol, 66 mg) were added into the mixture of Et_3N (30 mg) and ethylene glycol (5 mL) and refluxed for 24 h. The solid was filtered to afford the orange-red solid (21 mg, 25%). ^{1}H-NMR (400 MHz, DMSO, δ, ppm): 12.31 (s, 1H), 8.28 (d, J = 7.5 Hz, 1H), 8.18 (d, J = 6.7 Hz, 2H), 7.97–7.75 (m, 6H), 7.57 (t, J = 11.5 Hz, 1H), 7.45 (dt, J = 19.2, 6.8 Hz, 4H), 7.20 (d, J = 32.1 Hz, 3H), 6.86 (s, 2H), 6.81–6.68 (m, 3H), 6.64 (d, J = 7.3 Hz, 1H).

Preparation of IrBDP NPs

First, the IrBDP (0.2 mg) was dissolved in acetone (1 mL) and then the solution was added dropwise to distilled water (5 mL) with vigorous stirring. After the acetone was evaporated, the solution was dialyzed against water to obtain the IrBDP NPs.

ROS generation of IrBDP NPs

To evaluate the singlet oxygen generation ability, 1,3-diphenylisobenzofuran (DPBF) and indocyanine green (ICG) were used as indicator; their absorbance was monitored by absorption spectroscopy. The absorbance of DPBF in DMF and ICG in water were adjusted around 1, then IrBDP (0.8 μg·mL^{-1}) in DMF or IrBDP NPs were added. Their absorbance was monitored by absorption spectroscopy upon irradiation (16 mW·cm^{-2}, 530 nm).

Cell Imaging and Flow Cytometry

The Human cervical carcinoma (HeLa) cells were cultured in Dulbecco's modified Eagle's medium (DMEM, GIBCO) containing 10% fetal bovine serum (FBS, GIBCO), 100 μg·mL^{-1} streptomycin and 100 U·mL^{-1} penicillin at 37 °C in a humidified incubator containing 5% CO_2 and 95% air. After the HeLa cells were cultured for 24 h, the nanoparticles (2 μg·mL^{-1}) were added and the cells were respectively cultured for another 0.5 and 2 h for CLSM. Meanwhile, the HeLa cells were cultured for 24 h, the nanoparticles (2 μg·mL^{-1}) were added and the cells were cultured for 2 h. Then the media was replaced by the media containing the Lyso-tracker Red (1 μmol·L^{-1}) and the cells were incubated for another 30 min in 37 °C. The cell nuclei were stained by 4′,6-diamidino-2-phenyl-indole (DAPI). The

https://doi.org/10.1007/s10118-018-2096-9

result of flow cytometry was obtained by flow cytometer according to the treatment of cell imaging. (The IrBDP NPs channel: excitation wavelength, 488 nm; emission band-pass, 500−550 nm. The Lyso-tracker channel: excitation wavelength, 555 nm; emission band-pass, 590−650 nm).

Intracellular ROS Detection

The CLSM observation method was also employed to detect the ROS generation. First, HeLa cells were incubated with IrBDP NPs (2 μg·mL^{-1}) for 4 h upon irradiation (530 nm, 16 mW·cm^2) for 30 min, and then the culture medium was replaced and washed three times. Then, the DMEM containing dichlorofluorescin diacetate (DCFH-DA) (10^{-5} mol·L^{-1}) was added and further incubated for 30 min. The outcomes were observed with CLSM as soon as possible (excitation wavelength, 488 nm; emission band-pass, 500−550 nm).

MTT Assay

HeLa and CT26 cells harvested were seeded in 96-well plates with a density of 10^5 cells in every well and cultured in DMEM for 24 h. The medium was replaced by IrBDP NPs at a final concentration respectively. After incubation at 37 °C for 24 h about phototoxicity, the medium was replaced by the new medium with the MTT and cultured for another 4 h. The medium was removed and followed the addition of 150 μL of DMSO. The absorbance wavelength was set at 490 nm to measure the results by a microplate reader.

Calcein-AM/PI Test

To visually demonstrate the efficiency of IrBDP NPs in photodynamic therapy, the CT26 cells and HeLa cells were stained with propidium iodide and calcein-AM to identify dead (red) and live (green) cells, respectively. The control and drug-treated (0.1 μg·mL^{-1}) cells were incubated at 37 °C for 24 h in a humidified atmosphere containing 5% CO_2. Then, all dishes of cells were irradiated for 30 min with an LED light with a wavelength of 530 nm at an intensity of 16 mW·cm^{-2}. The cells were further incubated at 37 °C for another 24 h. After stained with calcein-AM/PI for 40 min and washed with phosphate-buffered saline (PBS), the two samples of cells were imaged with fluorescence microscopy.

Cell Apoptosis and Necrosis by Annexin V Staining

The apoptosis and necrosis induced by PDT of IrBDP NPs were evaluated by flow cytometry. HeLa cells were seeded at 1 × 10^6 cells/well in 6-well plates and further cultured for another 24 h. Then, the culture media were replaced by 1 mL of fresh culture media containing 10% FBS. IrBDP NPs were added into the cells, at a concentration of 2 μg·mL^{-1}. Cells incubated with PBS served as a blank control. After 4 h of incubation, the cells were irradiated with LED light (530 nm) at 16 mW·cm^{-2} for 40 min. Following incubation of 24 h, the floating dead cells and adherent alive cells were all collected and stained with propidium iodide (PI) and an Annexin V-FITC apoptosis detection kit according to the manufacturer's instructions. The apoptosis and necrosis results were examined on a flow cytometer.

RESULTS AND DISCUSSION

Synthesis and Characterization

The synthesis procedure is shown in Scheme 2. The compound **a** was synthesised according to the previous literature[42] and the structure was confirmed by proton nuclear magnetic resonance (^{1}H-NMR) as shown in Fig. S1 (in electronic supplementary information, ESI). The signal at 10.19 ppm indicated that the aldehyde group was successfully introduced. Subsequently, the compound BDP was synthesised and validated by ^{1}H-NMR as shown in Fig. S2 (in ESI). The signal at 5.99 ppm was the characteristic peak of BDP. Finally, the targeted compound IrBDP was synthesized and characterized by ^{1}H-NMR and matrix-assisted laser desorption/ion-ization time-of-flight mass spectrometry (MALDI-TOF MS). As shown in Figs. S3 and S5 (in ESI), the integration ratios of these peaks agreed well with those of theoretical calculations. The *m*/*z* signals located at 917.3 in the MALDI-TOF/TOF MS spectra is the same to the theoretical value of IrBDP. Meanwhile, in order to compare with the IrBDP, Ir-COOH was synthesized and used as the control (Fig. S4, in ESI).

Preparation and Characterization of IrBDP NPs

The self-assembly of organic molecules has been reported in previous work[43, 44]. Herein, we also attempted the preparation of IrBDP NPs *via* nanoprecipitation method. First, IrBDP was dissolved in acetone and then was added dropwise to distilled water under vigorous stirring. After dialysis against water, IrBDP NPs were obtained, and then characterized by transmission electron microscopy (TEM) and dynamic light scattering (DLS) as shown in Fig. 1. The average hydrodynamic diameter determined by DLS was about 190.2 nm, larger than the data obtained by TEM, which probably resulted from solvation effect and concentration dependence. As shown in Fig. 1(b), the size and size distribution showed negligible changes in the next week at room temperature, indicating high stability of IrBDP NPs in PBS.

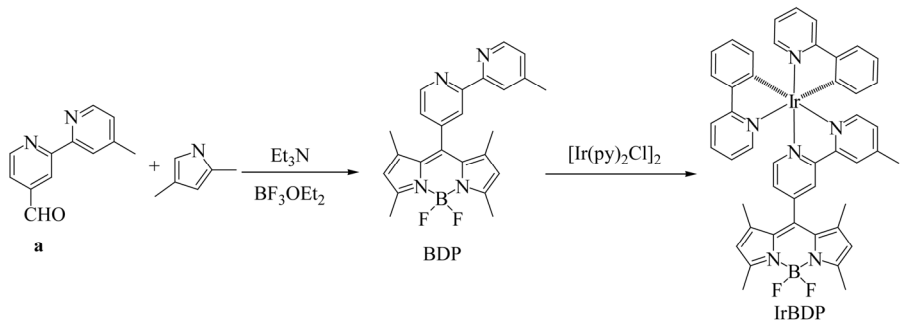

Scheme 2 The synthesis procedure of IrBDP

https://doi.org/10.1007/s10118-018-2096-9

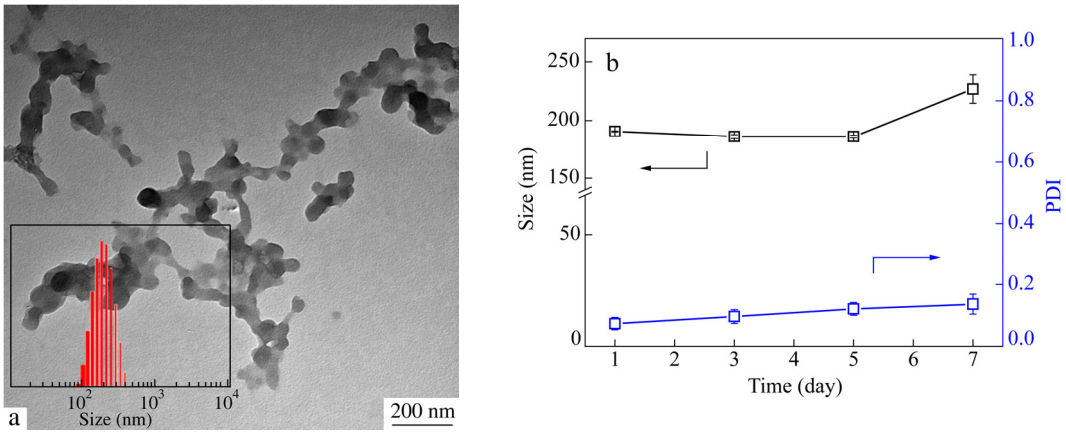

Fig. 1 (a) Transmission electron microscopy image of IrBDP NPs and (b) the stability in PBS over time (The inset in (a): Size and size distribution.)

The Study of Photophysical and Photochemical Properties

The photophysical properties were recorded by UV-Vis absorption and fluorescence emission spectra. Figure 2(a) shows the absorption spectra from 400 nm to 650 nm. The maximum absorption peak of BDP was at 502 nm. After introducing Ir to BDP, the absorption peak shifted to 507 nm maybe because of the heavy atom effect and the π-conjugation. Compared with the IrBDP, the maximum absorption peak of IrBDP NPs located at 520 nm, which bathochromic-shifted 13 nm. Figure 2(b) shows the fluorescence emission spectra of $[Ir(py)_2Cl]_2$, BDP, IrBDP and IrBDP NPs. The maximum emission peak of $[Ir(py)_2Cl]_2$ and BDP was at 523 and 532 nm, respectively. The maximum emission peak of IrBDP was at 526 nm, which fell in between the $[Ir(py)_2Cl]_2$ and BDP. After self-assembling in water, the maximum emission peak shifted to 554 nm (Fig. S6, in ESI). It is worthwhile to note that the fluorescence quantum yield of BDP decreased from 0.297 to 0.022 in virtue of the Ir(III) by

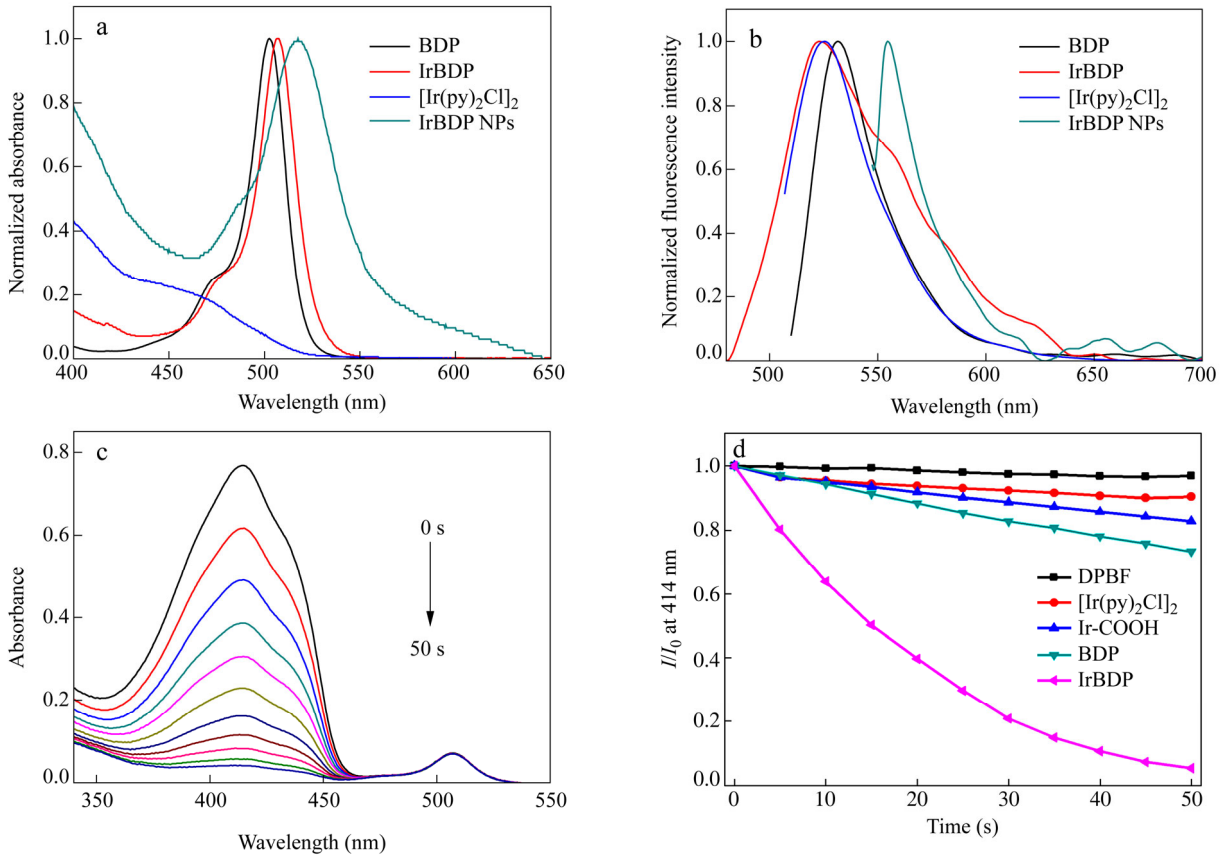

Fig. 2 The normalized (a) absorbance and (b) fluorescence spectra of BDP (THF, λ_{ex} = 500 nm), $[Ir(py)_2Cl]_2$ (THF, λ_{ex} = 450 nm), IrBDP (THF, λ_{ex} = 507 nm) and IrBDP NPs (H_2O, λ_{ex} = 518 nm); (c) Time-dependent absorption spectra of IrBDP upon irradiation (16 mW·cm^{-2}, 530 nm) in the presence of IrBDP in DMF; (d) Comparison of the decay rate of DPBF alone and of DPBF in the presence of free $[Ir(py)_2Cl]_2$, Ir-COOH, BDP and IrBDP, respectively

https://doi.org/10.1007/s10118-018-2096-9

using rhodamine 6G as the reference. These results confirm the formation of BDP@Ir complexes. In order to study the photodynamic effect of IrBDP, the photochemical properties were further investigated. The DPBF, which is a kind of singlet oxygen detection reagent, was used to detect the $^1O_2$ by time-dependent spectroscopy. DPBF itself caused negligible absorbance changes at 414 nm in 50 s under irradiation as shown in Fig. S7(a) (in ESI) and Fig. 2(d). Upon the addition of IrBDP (0.8 μg·mL^{-1}) in DMF, as expected, the absorbance at 414 nm decreased significantly, indicating an efficient degradation of DPBF in Figs. 2(c) and 2(d). According to the previous results[21], the BDP itself possesses photodynamic effect. Thus, the control experiments (BDP, Ir-COOH and $[Ir(py)_2Cl]_2$) were conducted and used to compare with the photodynamic effect of IrBDP. The solution of DPBF was irradiated in the presence of BDP, Ir-COOH and $[Ir(py)_2Cl]_2$ at the concentration of 2.5 μg·mL^{-1} in DMF, respectively. The $[Ir(py)_2Cl]_2$ (Fig. S7b, in ESI), Ir-COOH (Fig. S7c, in ESI) and BDP (Fig. S7d, in ESI) possessed weaker photodynamic effect compared with IrBDP even though the concentration of $[Ir(py)_2Cl]_2$, Ir-COOH and BDP was three times of IrBDP. This result indicated that the introduction of Ir significantly increased the photodynamic effect because of heavy atom effect. The photodynamic effect of IrBDP NPs was also assessed by detecting the decay rate of ICG. As shown in Fig. S8 (in ESI), the IrBDP NPs also possessed the comparable photodynamic effect.

The Investigation in Cells

The cellular uptake of IrBDP NPs in HeLa cells was investigated by using CLSM and flow cytometry. 4′,6-Diamidino-2-phenyl-indole (DAPI) was used to stain the cellular nuclei. As shown in Fig. 3(a), IrBDP was not observed in the cellular nuclei. Nearly all cells can internalize the IrBDP NPs, and the IrBDP NPs located abundantly in the cytoplasm of the HeLa cells. The fluorescence of IrBDP increased with incubation time from 0.5 h to 2 h, and the enhanced cellular uptake of IrBDP NPs was also confirmed by flow cytometry (Fig. 3b). To have insight into the fate of

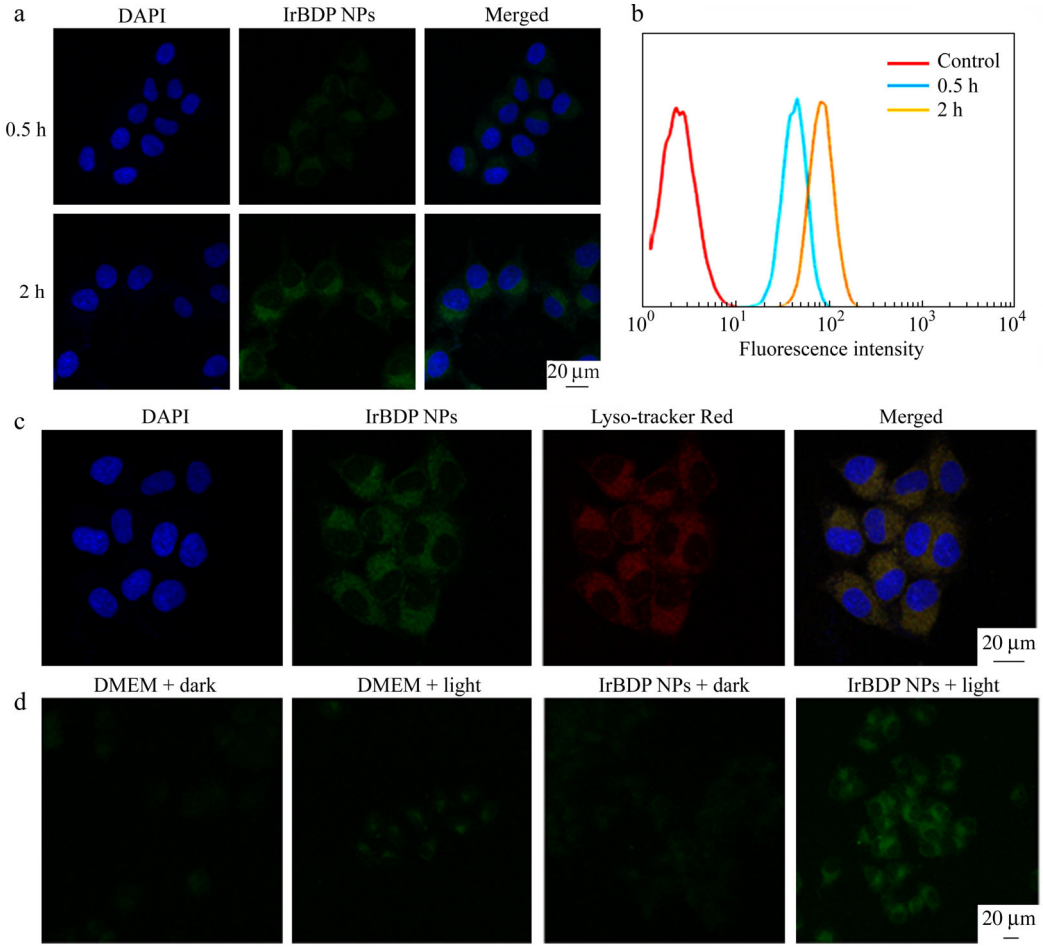

Fig. 3 (a) Fluorescence microscopy images of HeLa cells incubated with IrBDP (2 μg·mL^{-1}) for 0.5 and 2 h at 37 °C; (b) Quantitative analysis of HeLa cells incubated with IrBDP NPs (2 μg·mL^{-1}) for 0.5 and 2 h at 37 °C using the flow cytometry with cells untreated as a control; (c) CLSM images of HeLa cells costained with IrBDP NPs (2 μg·mL^{-1}) and Lyso-tracker Red (The images showed the fluorescence of nuclei (blue), IrBDP NPs (green), Lyso-tracker Red (red) and merged images (yellow) from left to right.); (d) The generation of intracellular ROS mediated by IrBDP NPs samples upon light irradiation of 16 mW·cm^{-2} for 20 min indicated by the fluorescence of DCF about the DMEM control, DMEM with light, IrBDP NPs and IrBDP NPs upon irradiation treatment (The IrBDP NPs channel: excitation wavelength, 488 nm; emission band-pass, 500−550 nm. the Lyso-tracker channel: excitation wavelength, 555 nm; emission band-pass, 590−650 nm. The inset in a, c, d: scale bar = 20 μm) (The online verion is colorful.)

https://doi.org/10.1007/s10118-018-2096-9

IrBDP NPs internalized by cells, colocalization experiment was conducted with a commercially available Lyso-tracker Red in HeLa cells. HeLa cells were pretreated with IrBDP NPs (2 μg·mL^{-1}) for 1 h and then stained with Lyso-tracker Red (1 μmol·L^{-1}) at 37 °C. As shown in Fig. 3(c), the fluorescence of IrBDP NPs (green) superimposed with the fluorescence of Lyso-tracker Red (red) and produced an orange fluorescence in the merged images, revealing the receptor-mediated endocytosis. To verify that the IrBDP NPs could generate singlet oxygen in HeLa cells, the DCFH-DA was used as the indicator. As shown in Fig. 3(d), negligible green fluorescence was observed in all control groups because there is no adequate singlet oxygen to oxidize nonfluorescent DCFH-DA into fluorescent dichlorofluorescein (DCF). On the contrary, a bright green fluorescence emerged in IrBDP NPs upon irradiation group. The result indicated that the IrBDP NPs could generate effectively singlet oxygen in HeLa cells and could be used as photodynamic agent.

The phototoxicity of IrBDP NPs was investigated *via* 3-(4,5-dimethylthiazol-2-yl)-2,5diphenyltetraz-oliumbromide (MTT) colorimetric assay for 24 h. Figures 4(a) and 4(b) show the cell viability of CT26 and HeLa when incubated with IrBDP NPs, respectively. IrBDP NPs in dark did not induce obvious cell death. In contrast, IrBDP NPs showed the potent phototoxicity and the cell viability significantly decreased in a dose-dependent manner upon irradiation. In

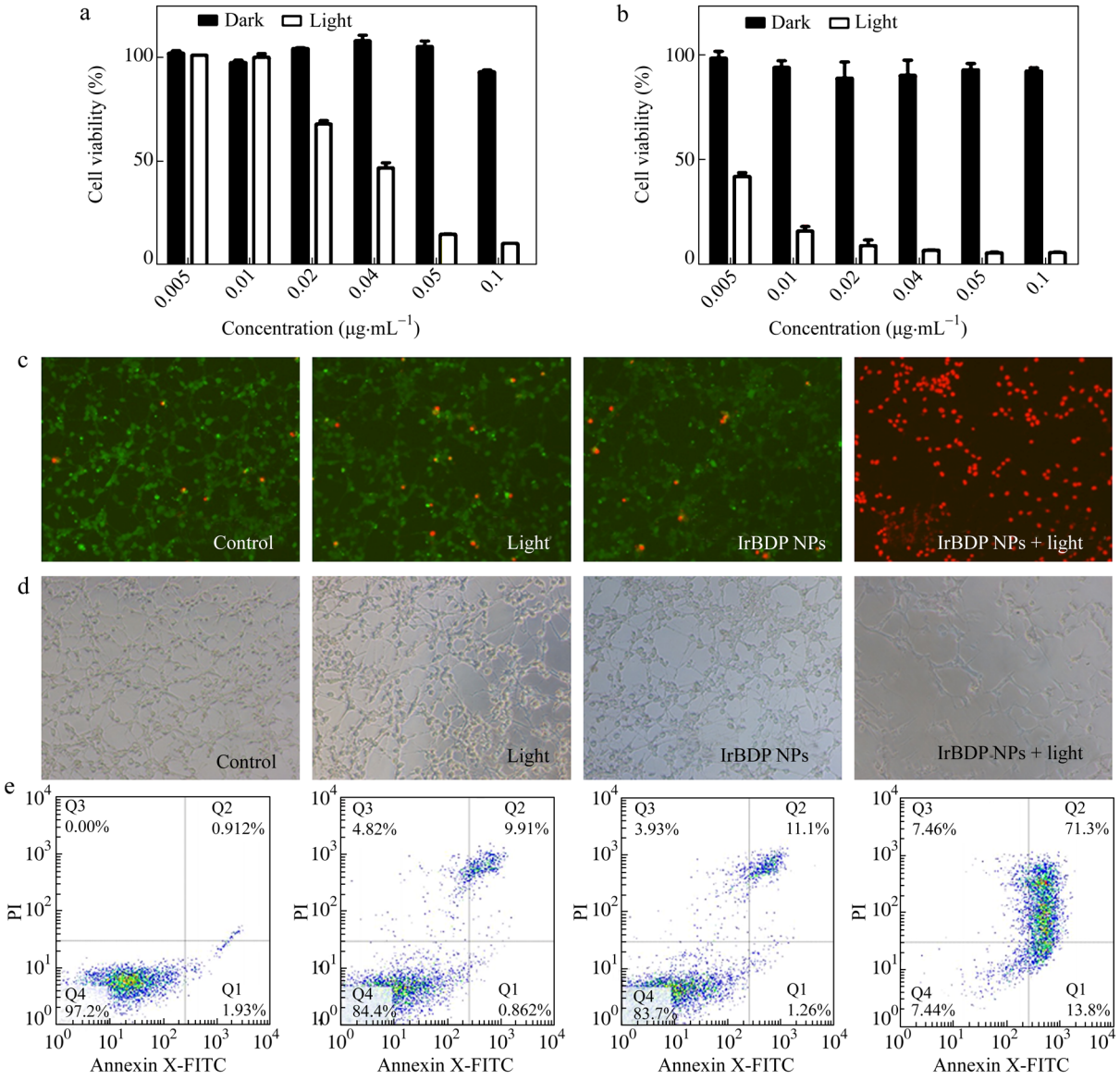

Fig. 4 Cell viability of (a) CT26 and (b) HeLa incubated with IrBDP NPs for 4 h at 37 °C upon irradiation (16 mW·cm^{-2}, 530 nm) for 30 min and culture another 24 h; (c) Fluorescence images of calcein AM (green, live cells) and propidium iodide (red, dead cells) co-stained and (d) the bright field photos of CT26 cells (from left to right: blank, irradiation, IrBDP NPs without irradiation and IrBDP NPs upon irradiation (CT26 cells incubated for 24 h with the IrBDP NPs at the concentration of 0.1 μg·mL^{-1} after irradiation (16 mW·cm^{-2}, 530 nm) for 30 min at 37 °C); (e) Flow cytometry analysis of CT26 cells (from left to right: blank, only irradiation, IrBDP NPs (2 μg·mL^{-1}) without irradiation and IrBDP NPs (2 μg·mL^{-1}) upon irradiation. The four areas represent the different phases of the cells: necrotic (Q1), late-stage apoptotic (Q2), early apoptotic (Q3), and live (Q4).) (The online version is colorful.)

https://doi.org/10.1007/s10118-018-2096-9

addition, the live/dead staining experiment was carried out to validate that the cell apoptosis and necrosis were triggered by irradiation. As shown in Fig. 4(c), almost all of the CT26 cells emit plentiful green fluorescence in all control groups. Meanwhile, after incubated with IrBDP NPs under irradiation, a majority of cells were dead with strong red fluorescence. Simultaneously, the CT26 cells were treated with the same condition and the bright field photos were obtained. As shown in Fig. 4(d), nearly all the cells were healthy and the morphology of cells was in good condition in all control groups. The morphology of cells treated with IrBDP NPs under irradiation was broken and cracked. The HeLa cells also indicated the similar results in Figs. S9(a) and S9(b) (in ESI). In order to further demonstrate the cell death mechanism, the cells apoptosis experiment was conducted. CT26 cells were double-labeled with Annexin V-FITC (fluoresceine isothiocyanate) and PI (propidium iodide) before flow cytometry analysis. As shown in Fig. 4(e), compared with the control groups, the cell apoptotic rate (Q2 + Q3) was significantly increased to 85.1% from 12.36% under treatment with IrBDP NPs upon irradiation. The HeLa cells were also subjected to the cells apoptosis experiment. As shown in Fig. S9(c), the cell apoptotic rate (Q2 + Q3) significantly increased to 69.8% from 2.555%. These results manifest that the IrBDP NPs possess excellent photodynamic effect *in vitro* and can be used as photodynamic therapy agent.

CONCLUSIONS

In summary, the fluorescent cyclometalated Ir(III) complex IrBDP was successfully synthesized, which could self-assemble into nanoparticles. The resulting IrBDP NPs could be engulfed by cells for cell imaging. The introduction of Ir(III) obviously increased the photodynamic effect, and resulted in enhanced cell death and apoptosis. This work provides a useful approach to develop a new and potential photosensitizer for PDT.

Electronic Supplementary Information

Electronic supplementary information (ESI) is available free of charge in the online version of this article at: https://doi.org/10.1007/s10118-018-2096-9.

ACKNOWLEDGMENTS

This work was financially supported by the National Natural Science Foundation of China (Nos. 21474012 and 21504089).

REFERENCES

1 Li, H.; Wang, P.; Deng, Y.; Zeng, M.; Tang, Y.; Zhu, W. H.; Cheng, Y. Combination of active targeting, enzyme-triggered release and fluorescent dye into gold nanoclusters for endomicroscopy-guided photothermal/photodynamic therapy to pancreatic ductal adenocarcinoma. Biomaterials 2017, 139, 30–38.
2 Li, X.; Gao, M.; Xin, K.; Zhang, L.; Ding, D.; Kong, D.; Wang, Z.; Shi, Y.; Kiessling, F.; Lammers, T.; Cheng, J.; Zhao, Y. Singlet oxygen-responsive micelles for enhanced photodynamic therapy. J. Control. Release 2017, 260, 12–21.
3 Linares, I. A. P.; de Oliveira, K. T.; Perussi, J. R. Chlorin derivatives sterically-prevented from self-aggregation with high antitumor activity for photodynamic therapy. Dyes Pigm. 2017, 145, 518–527.
4 Xiong, H.; Zhou, D.; Zheng, X.; Qi, Y.; Wang, Y.; Jing, X.; Huang, Y. Stable amphiphilic supramolecular self-assembly based on cyclodextrin and carborane for the efficient photodynamic therapy. Chem. Commun. 2017, 53, 3422–3425.
5 Du, E.; Hu, X.; Roy, S.; Wang, P.; Deasy, K.; Mochizuki, T.; Zhang, Y. Taurine-modified Ru(ii)-complex targets cancerous brain cells for photodynamic therapy. Chem. Commun. 2017, 53, 6033–6036.
6 Gu, B.; Wu, W.; Xu, G.; Feng, G.; Yin, F.; Chong, P. H. J.; Qu, J.; Yong, K. T.; Liu, B. Precise two-photon photodynamic therapy using an efficient photosensitizer with aggregation-induced emission characteristics. Adv. Mater. 2017, 29(28), DOI: 10.1002/adma.201701076
7 Huang, L.; Li, Z.; Zhao, Y.; Yang, J.; Yang, Y.; Pendharkar, A. I.; Zhang, Y.; Kelmar, S.; Chen, L.; Wu, W.; Zhao, J.; Han, G. Enhancing photodynamic therapy through resonance energy transfer constructed near-Infrared photosensitized nanoparticles. Adv. Mater. 2017, 29(28), DOI: 10.1002/adma.201604789
8 Yue, C.; Yang, Y.; Song, J.; Alfranca, G.; Zhang, C.; Zhang, Q.; Yin, T.; Pan, F.; de la Fuente, J. M.; Cui, D. Mitochondria-targeting near-infrared light-triggered thermosensitive liposomes for localized photothermal and photodynamic ablation of tumors combined with chemotherapy. Nanoscale 2017, 9, 11103–11118.
9 Zheng, Y.; Lu, H.; Jiang, Z.; Guan, Y.; Zou, J.; Wang, X.; Cheng, R.; Gao, H. Low-power white light triggered AIE polymer nanoparticles with high ROS quantum yield for mitochondria-targeted and image-guided photodynamic therapy. J. Mater. Chem. B 2017, 5, 6277–6281.
10 Li, Y.; Zheng, X.; Zhang, X.; Liu, S.; Pei, Q.; Zheng, M.; Xie, Z. Porphyrin-based carbon dots for photodynamic therapy of hepatoma. Adv. Healthc. Mater. 2017, 6(1), DOI: 10.1002/adhm.201600924
11 Liu, W.; Wang, Y. M.; Li, Y. H.; Cai, S. J.; Yin, X. B.; He, X. W.; Zhang, Y. K. Fluorescent imaging-guided chemotherapy-and-photodynamic dual therapy with nanoscale porphyrin metal-organic framework. Small 2017, 13(17), DOI: 10.1002/smll.201603459
12 Rui, L.; Xue, Y.; Wang, Y.; Gao, Y.; Zhang, W. A mitochondria-targeting supramolecular photosensitizer based on pillararene for photodynamic therapy. Chem. Commun. 2017, 53, 3126–3129.
13 Zhang, W.; Lin, W.; Zheng, X.; He, S.; Xie, Z. Comparing effects of redox sensitivity of organic nanoparticles to photodynamic activity. Chem. Mater. 2017, 29, 1856–1863.
14 Zheng, X.; Wang, L.; Pei, Q.; He, S.; Liu, S.; Xie, Z. Metal-organic framework@porous organic polymer nanocomposite for photodynamic therapy. Chem. Mater. 2017, 29, 2374–2381.
15 Isik, M.; Guliyev, R.; Kolemen, S.; Altay, Y.; Senturk, B.; Tekinay, T.; Akkaya, E. U. Designing an intracellular fluorescent probe for glutathione: two modulation sites for selective signal transduction. Org. Lett. 2014, 16, 3260–3263.
16 Isik, M.; Ozdemir, T.; Turan, I. S.; Kolemen, S.; Akkaya, E. U. Chromogenic and fluorogenic sensing of biological thiols in aqueous solutions using BODIPY-based reagents. Org. Lett. 2013, 15, 216–219.
17 Göl, C.; Malkoç, M.; Yeşilot, S.; Durmuş, M. Novel zinc(II) phthalocyanine conjugates bearing different numbers of BODIPY and iodine groups as substituents on the periphery.

Dyes Pigm. 2014, 111, 81–90.
18 Kim, B.; Sui, B.; Yue, X.; Tang, S.; Tichy, M. G.; Belfield, K. D. *In vitro* photodynamic studies of a BODIPY-based photosensitizer. Eur. J. Org. Chem. 2017, (1), 25–28.
19 Wang, W.; Wang, L.; Li, Z.; Xie, Z. BODIPY-containing nanoscale metal-organic frameworks for photodynamic therapy. Chem. Commun. 2016, 52, 5402–5405.
20 Guo, Z.; Zou, Y.; He, H.; Rao, J.; Ji, S.; Cui, X.; Ke, H.; Deng, Y.; Yang, H.; Chen, C.; Zhao, Y.; Chen, H. Bifunctional platinated nanoparticles for photoinduced tumor ablation. Adv. Mater. 2016, 46(28), 10155–10164.
21 Liu, Y.; Li, Z.; Chen, L.; Xie, Z. Near infrared BODIPY-platinum conjugates for imaging, photodynamic therapy and chemotherapy. Dyes Pigm. 2017, 141, 5–12.
22 Cakmak, Y.; Kolemen, S.; Duman, S.; Dede, Y.; Dolen, Y.; Kilic, B.; Kostereli, Z.; Yildirim, L. T.; Dogan, A. L.; Guc, D.; Akkaya, E. U. Designing excited states: theory-guided access to efficient photosensitizers for photodynamic action. Angew. Chem. 2011, 50, 11937–11941.
23 Epelde-Elezcano, N.; Palao, E.; Manzano, H.; Prieto-Castaneda, A.; Agarrabeitia, A. R.; Tabero, A.; Villanueva, A.; de la Moya, S.; Lopez-Arbeloa, I.; Martinez-Martinez, V.; Ortiz, M. J. Rational design of advanced photosensitizers based on orthogonal BODIPY dimers to finely modulate singlet oxygen generation. Chem. Eur. J. 2017, 23, 4837–4848.
24 Ozdemir, T.; Bila, J. L.; Sozmen, F.; Yildirim, L. T.; Akkaya, E. U. Orthogonal Bodipy trimers as photosensitizers for photodynamic action. Org. Lett. 2016, 18, 4821–4823.
25 Wu, W.; Cui, X.; Zhao, J. Hetero BODIPY-dimers as heavy atom-free triplet photosensitizers showing a long-lived triplet excited state for triplet-triplet annihilation upconversion. Chem. Commun. 2013, 49, 9009–9011.
26 Zhang, X. F.; Yang, X. Photosensitizer that selectively generates singlet oxygen in nonpolar environments: photophysical mechanism and efficiency for a covalent BODIPY dimer. J. Phys. Chem. B 2013, 117, 9050–9055.
27 Mari, C.; Huang, H.; Rubbiani, R.; Schulze, M.; Würthner, F.; Chao, H.; Gasser, G. Evaluation of perylene bisimide-based RuIIand IrIII complexes as photosensitizers for photodynamic therapy. Eur. J. Inorg. Chem. 2017, 2017, 1745–1752.
28 Wang, L.; Yin, H.; Cui, P.; Hetu, M.; Wang, C.; Monro, S.; Schaller, R. D.; Cameron, C. G.; Liu, B.; Kilina, S.; McFarland, S. A.; Sun, W. Near-infrared-emitting heteroleptic cationic iridium complexes derived from 2,3-diphenylbenzo [*g*]quinoxaline as *in vitro* theranostic photodynamic therapy agents. Dalton Trans. 2017, 46, 8091–8103.
29 Xiang, H.; Chen, H.; Tham, H. P.; Phua, S. Z. F.; Liu, J. G.; Zhao, Y. Cyclometalated iridium(III)-complex-based micelles for glutathione-responsive targeted chemotherapy and photodynamic therapy. ACS Appl. Mater. Interfaces 2017, 9, 27553–27562.
30 Zheng, Y.; He, L.; Zhang, D. Y.; Tan, C. P.; Ji, L. N.; Mao, Z. W. Mixed-ligand iridium(iii) complexes as photodynamic anticancer agents. Dalton Trans. 2017, 46, 11395–11407.
31 Liu, J.; Jin, C.; Yuan, B.; Liu, X.; Chen, Y.; Ji, L.; Chao, H. Selectively lighting up two-photon photodynamic activity in mitochondria with AIE-active iridium(iii) complexes. Chem. Commun. 2017, 53, 2052–2055.
32 McKenzie, L. K.; Sazanovich, I. V.; Baggaley, E.; Bonneau, M.; Guerchais, V.; Williams, J. A.; Weinstein, J. A.; Bryant, H. E. Metal complexes for two-photon photodynamic therapy: a cyclometallated iridium complex induces two-photon photosensitization of cancer cells under near-IR light. Chem. Eur. J. 2017, 23, 234–238.
33 Nam, J. S.; Kang, M. G.; Kang, J.; Park, S. Y.; Lee, S. J.; Kim, H. T.; Seo, J. K.; Kwon, O. H.; Lim, M. H.; Rhee, H. W.; Kwon, T. H. Endoplasmic reticulum-localized iridium(III) complexes as efficient photodynamic therapy agents *via* protein modifications. J. Am. Chem. Soc. 2016, 138, 10968–10977.
34 Qiu, K.; Ouyang, M.; Liu, Y.; Huang, H.; Liu, C.; Chen, Y.; Ji, L.; Chao, H. Two-photon photodynamic ablation of tumor cells by mitochondria-targeted iridium(iii) complexes in aggregate states. J. Mater. Chem. B 2017, 5, 5488–5498.
35 Tian, X.; Zhu, Y.; Zhang, M.; Luo, L.; Wu, J.; Zhou, H.; Guan, L.; Battaglia, G.; Tian, Y. Localization matters: a nuclear targeting two-photon absorption iridium complex in photodynamic therapy. Chem. Commun. 2017, 53, 3303–3306.
36 Deligonul, N.; Browne, A. R.; Golen, J. A.; Rheingold, A. L.; Gray, T. G. Cyclometalated iridium(III) complexes of azadipyrromethene chromophores. Organometallics 2014, 33, 637–643.
37 Zhou, J.; Gai, L.; Zhou, Z.; Mack, J.; Xu, K.; Zhao, J.; Qiu, H.; Chan, K. S.; Shen, Z. Highly efficient near IR photosensitizers based on Ir—C bonded porphyrin-aza-BODIPY conjugates. RSC Adv. 2016, 6, 72115–72120.
38 Majumdar, P.; Yuan, X.; Li, S.; Le Guennic, B.; Ma, J.; Zhang, C.; Jacquemin, D.; Zhao, J. Cyclometalated Ir(iii) complexes with styryl-BODIPY ligands showing near IR absorption/emission: preparation, study of photophysical properties and application as photodynamic/luminescence imaging materials. J. Mater. Chem. B 2014, 2, 2838–2854.
39 Palao, E.; Sola-Llano, R.; Tabero, A.; Manzano, H.; Agarrabeitia, A. R.; Villanueva, A.; Lopez-Arbeloa, I.; Martinez-Martinez, V.; Ortiz, M. J. Acetylacetonate BODIPY-biscyclometalated iridium(III) complexes: effective strategy towards smarter fluorescent photosensitizer agents. Chem. Eur. J. 2017, 23, 10139–10147.
40 Sun, J.; Zhong, F.; Yi, X.; Zhao, J. Efficient enhancement of the visible-light absorption of cyclometalated Ir(III) complexes triplet photosensitizers with BODIPY and applications in photooxidation and triplet-triplet annihilation upconversion. Inorg. Chem. 2013, 52, 6299–6310.
41 Tabrizi, L.; Chiniforoshan, H. New cyclometalated Ir(iii) complexes with NCN pincer and meso-phenylcyanamide BODIPY ligands as efficient photodynamic therapy agents. RSC Adv. 2017, 7, 34160–34169.
42 Khairoutdinov, R. F.; Doubova, L. V.; Haddon, R. C.; Saraf, L. Persistent photoconductivity in chemically modified single-wall carbon nanotubes. J. Phys. Chem. B 2004, 108, 19976–19981.
43 Li, Z.; Zheng, M.; Guan, X.; Xie, Z.; Huang, Y.; Jing, X. Unadulterated BODIPY-dimer nanoparticles with high stability and good biocompatibility for cellular imaging. Nanoscale 2014, 6, 5662–5665.
44 Liu, Y.; Song, N.; Chen, L.; Xie, Z. Triple-BODIPY organic nanoparticles with particular fluorescence emission. Dyes Pigm. 2017, 147, 241–245.

https://doi.org/10.1007/s10118-018-2096-9